



Wireless electroanalysis of mycotoxins with hybrid light-emitting devices based on molecularly imprinted polymers

Tamara Moya-Cavas^a, Leslie R. Arias-Aranda^b, Elena Benito-Peña^a, Laurent Bouffier^b, Neso Sojic^b, Gerardo Salinas^{b,*}, Guillermo Orellana^{c,*}

^a Department of Analytical Chemistry, Faculty of Chemistry, Plaza de las Ciencias 2, Complutense University of Madrid, Madrid E-28040, Spain

^b Univ. Bordeaux, CNRS, Bordeaux INP, ISM, UMR 5255, Pessac F-33607, France

^c Department of Organic Chemistry, Faculty of Chemistry, Plaza de las Ciencias 2, Complutense University of Madrid, Madrid E-28040, Spain

ARTICLE INFO

Keywords:

Bipolar electrochemistry
Molecularly imprinted polymer
Zearalenone
Light-emitting diode
Mycotoxins
Food analysis

ABSTRACT

Molecularly imprinted polymers (MIPs) act as “artificial antibodies” offering molecular recognition along with advantages like cost-effective production, versatility, stability, and reusability. These features make MIPs ideal for detecting food contaminants such as mycotoxins, harmful secondary metabolites produced by fungi on cereals, fruits, and vegetables. However, their use as sensors requires a transducer of the analyte binding event. In this work, we report the development of a hybrid light-emitting device for the wireless electroanalysis of zearalenone (ZON), as exemplary mycotoxin with endocrine disrupting activity. Our approach combines the concepts of bipolar electrochemistry (BE) with the fine molecular recognition of a tailored MIP and the optical readout provided by a light-emitting diode (LED). The polymeric-microelectronic hybrid bipolar electrode incorporates a MIP-coated anode and a gold wire cathode to the extremities of a green LED. The MIP responds immediately to the binding of the target mycotoxin, facilitating redox reactions of the electroactive probe ($[\text{Fe}(\text{CN})_6]^{3-/4-}$) at each terminal of the bipolar electrode and triggering the emission of light. A correlation between the intensity of the emitted light and the analyte concentration was obtained. By integrating the BE setup with a microfluidic platform, a highly sensitive analytical device has been built, offering a linear ZON quantification range of 10–70 ng mL⁻¹, suitable for its quantification in food samples.

1. Introduction

Molecularly imprinted polymers (MIPs) have represented a significant innovation in the field of analytical chemistry, offering a synthetic alternative to biological antibodies [1–3]. Briefly, MIPs are produced via polymerization of functional monomers in the presence of a template molecule, which defines the specific recognition features of the material. After the synthesis, the template molecule is removed, leaving cavities within the polymer matrix that match the template in size, shape, and functional groups. This endows MIPs with molecular recognition capabilities akin to those of their biological peers, with the advantages of enhanced chemical, thermal, and mechanical stability, as well as reusability. Recently, MIPs have been successfully used for the chemical analysis of pesticides, metal ions, pathogenic bacteria and mycotoxins [1,4–8]. In particular, the latter are toxic secondary metabolites produced by fungi that contaminate a wide range of agricultural products such as cereals, fruits, and vegetables [9]. In this context, different

specific MIPs for the detection of mycotoxins such as zearalenone (ZON), aflatoxin B1, ochratoxin A, and deoxynivalenol (DON), have been realized [10–13]. ZON, an estrogenic metabolite produced by *Fusarium* fungi, poses a significant risk to human and animal health alike [14]. It has been found that nearly 60 % of all food samples analyzed worldwide contain ZON; therefore, the development of accurate and straightforward methods of quantification of this mycotoxin is of high interest [15].

The significant affinity and selectivity of MIPs have been extensively used in multiple analytical techniques, ranging from chromatographic systems to optochemical and electrochemical sensors [16–19]. However, most of them face limitations, often requiring expensive equipment, lengthy procedures or direct electrical connections that may hinder their application. A promising alternative that addresses some of those limitations exploits the inherent advantages of bipolar electrochemistry (BE), such as simplified equipment, shorter processing times and adaptability to *in vivo* applications [20–24]. BE is based on the induction

* Corresponding authors.

E-mail addresses: Gerardo.salinassanchez@enscbp.fr (G. Salinas), gorellana@ucm.es (G. Orellana).

<https://doi.org/10.1016/j.snb.2025.137566>

Received 13 December 2024; Received in revised form 28 February 2025; Accepted 3 March 2025

Available online 4 March 2025

0925-4005/© 2025 Elsevier B.V. All rights reserved, including those for text and data mining, AI training, and similar technologies.

of a polarization potential difference (ΔV) across a conducting substrate or “bipolar electrode” (BPE) by applying an external electric field (E) [20–22]. When ΔV overcomes the thermodynamic threshold potential (ΔV_{min}) established for a set of electroactive species, redox reactions take place asymmetrically at each extremity of the BPE. Due to its operational simplicity, BE has become a powerful tool in multiple applications ranging from material science and environmental remediation to organic electrosynthesis [25–27]. BE has emerged recently as an interesting alternative to generate unconventional dynamic and optical readouts of chemical information in electroanalysis [28–36]. The latter show multiple advantages such as high sensitivity, broad dynamic range, short response time and low cost [37–41]. The use of optoelectronic devices such as light-emitting diodes (LEDs) has gained considerable attention in electroanalysis since, in contrast to alternative light-emitting techniques such as fluorescence and electrochemiluminescence, no additional light sources and chemicals are required [42–46]. Interestingly, the chemical information associated to the redox reactions in BE is encoded in the electron flux travelling from the anode to the cathode of the BPE [47]. Hence, LEDs represent stable and controllable light sources that can generate optical signals in response to molecular recognition events [48]. Moreover, unlike electrochemical readouts, the emission of light from LEDs is related to the charge carrier mobilities (electrons and holes), triggered by an external electric stimulus; therefore, small changes of current result in large variations of the luminous intensity. Furthermore, the LED transduction can readily be used as an optical alarm to warn on the mycotoxin level in the sample above a set threshold.

In this work, we report an unconventional strategy for the sensitive quantification of ZON, based on the synergy between the molecular recognition ability of a MIP and a wireless optoelectronic readout powered by BE. The MIP was synthesized by thermal polymerization on the surface of a functionalized gold wire, with *N*-(2-aminoethyl) methacrylamide (EAMA) acting as functional monomer and cyclododecyl 2,4-dihydroxybenzoate (CDHB), a surrogate of ZON, as the template molecule. The use of a mimic rather than the target analyte has proven to be very useful for trace analysis because any bleeding from the MIP does not alter the low limit of detection. A surrogate is also valuable in those cases where the analyte cannot be used as template, due to its toxicity, high cost, and/or limited availability, as in the case of ZON.

These elements were selected for their capacity to form highly specific cavities for ZON recognition, improving the polymer selectivity [10]. The hybrid BPE is designed by combining three main components: (i) a selective MIP for the chemical target recognition, (ii) a micro-LED for the transducing emission of light, and (iii) gold wires connected to the terminals of the LED, where the redox reactions occur (Fig. 1). When

a high enough electric field is applied into the solution, reduction and oxidation of the $[\text{Fe}(\text{CN})_6]^{3-}$ and $[\text{Fe}(\text{CN})_6]^{4-}$ species, acting as a sacrificial redox pair, trigger a flux of electrons from the anode to the cathode of the hybrid BPE powering the emission of the LED. The MIP coating on one of the gold wires plays the role of a chemically-sensitive on-off switch, since the presence of ZON facilitates the electron-transfer reaction. The integration of MIPs with LEDs represents in this way a promising approach to develop highly sensitive and specific sensors that furnish a straightforward readout. This innovative approach has the potential to become an alternative tool for *in situ* food analysis, due to the synergy between the selectivity of MIPs and the analytical advantages of BE. With this research, we aim not only to advance in the field of mycotoxin detection but also to open new avenues for the development of streamlined sensors for a wide range of applications.

2. Materials and methods

2.1. Reactants and materials

Reactants for the synthesis of MIPs, solvents, buffers, toxins, surrogate, materials for manufacturing the BE cells, syntheses and purification protocols are fully described in the [Supporting Information](#).

2.2. Chemical modification of the gold electrode surface

The functionalization of the Au wire was carried out in a two-step procedure (Figure S1). Firstly, the metal surface was functionalized with amino groups by immersing a 1.0 cm-long segment of the wire in a 3 mmol L⁻¹ 6-amino-1-hexanethiol (Indagoo, 95 %) solution in absolute ethanol placed into a HPLC glass vial. The amount of solution controls the height of the functionalized segment because the gold wire is held tightly into a PFA tubing inserted into a rubber septum, while a segment of the wire protrudes out of the tubing. The wire was allowed to react overnight at 5 °C into the solution and then it was thoroughly rinsed with absolute ethanol and toluene. In a second step, the activated wire was transferred to a septum-capped 12-mL glass vial containing 14 mg of pre-dried potassium carbonate (K_2CO_3 , Scharlau) in anhydrous toluene. Then, dry argon sparging was set for 15 min before 240 μmol of acryloyl chloride (Merck, 96 %), dissolved in a small volume of anhydrous toluene, was introduced dropwise with a syringe. The reaction was kept at room temperature overnight under the inert atmosphere.

The MIP was prepared from a mixture of neutralized EAMA (8 μmol), methacrylamide (MAM, 8 μmol), CDHB (4 μmol), ethylene glycol dimethacrylate (EDMA, 14 μmol), and azobisisobutyronitrile (AIBN, 5 % of the total monomers weight) in 5 mL of dimethylsulfoxide (DMSO). The gold wire, functionalized with acrylamide groups, was dipped in this pre-polymerization mixture. The solution was then deoxygenated by argon sparging for 30 min, and polymerization was conducted in a thermostatic bath using the following temperature profile: 50 °C for 2 h, 65 °C overnight, and 80 °C for 2 h. After polymerization, the MIP-coated gold wire (Au@MIP) was thoroughly rinsed with DMSO to eliminate the excess of monomers. To remove the template molecule, the wire was washed for 30 min into 2 mL of a methanol–trifluoroacetic acid (TFA; 95:5 v/v) mixture with stirring, followed by washing with 2 mL of methanol for another 30 min. Non-imprinted polymers (NIPs) were prepared similarly but in the absence of the template molecule (Au@NIP). Those functionalization and polymerization procedures were also used to modify the gold disk electrodes (3 mm dia., Autolab). The morphology of the resultant polymers was characterized by scanning electron microscopy (SEM; JEOL JSM 7600 F) operating at 20 kV (UCM National Center for Electron Microscopy).

2.3. Electrochemical measurements

The classical electrochemistry measurements were performed in a three-electrode cell comprising an Au disk electrode, a platinum mesh

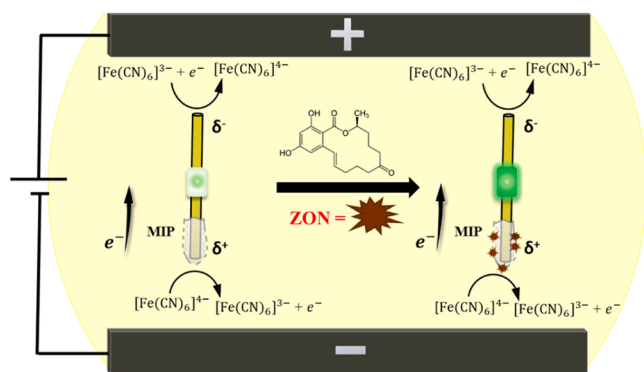


Fig. 1. Illustration of the hybrid MIP–bipolar system, in the absence (left) and in the presence of ZON (right), with a depiction of the associated redox reactions, the anodically and cathodically polarized gold wires (δ^+ and δ^- , respectively), and the resulting emission from the green LED in the presence of the mycotoxin when an appropriate electric field is applied between the feeder electrodes.

(99.9 % AlfaAesar), and a silver wire (99.9 %, 0.5 mm dia., AlfaAesar) as working, counter and pseudo-reference electrodes, respectively. All the potentiodynamic studies were carried out with a PalmSense® potentiostat connected to a personal computer. BE measurements were carried out into a 5 mmol L⁻¹ pH 8.2 phosphate buffer solution containing [Fe(CN)₆]³⁻ and [Fe(CN)₆]⁴⁻ (0.8 mmol L⁻¹ each) as redox probe. This electrolytic solution was used for all the measurements unless otherwise stated. In all the BE experiments a Manson EP-613 power supply coupled to an ARCELI ARC-1001 electronic voltage regulator were used.

2.4. BPE cells fabrication

The hybrid BPE was manufactured by connecting a pristine and the polymer-coated Au wires to the cathode and anode, respectively, of a miniature green LED (RS 654–4304 consisting of a green 0603 SMD LED on a 1.7 mm × 0.8 mm × 0.65 mm base). A small amount of silver paint (Electrode Microscopy Sciences) was employed to establish electric connection between the Au wires and the LED terminals.

2.4.1. Classical platform

The classical bipolar electrochemical cell was made up of the hybrid BPE, either the Au/LED/Au@MIP or the Au/LED/Au@NIP, positioned between two 2 mm dia. × 8.5 cm long graphite feeder electrodes (Staedtler, 2H) (Figure S2). In this cell a constant electric field of 1.16 V cm⁻¹ is applied between the two parallel feeder electrodes positioned 5.5 cm apart in a 9-cm plastic Petri dish. Several 1 – 27 µL aliquots of stock solutions of ZON are added to provide 0 – 100 ng mL⁻¹ of the mycotoxin in 30 mL of the electrolytic working solution. The medium is homogenized after each addition with the help of a 5 mL micropipette and then allowed to incubate for 5 min in order to permit the diffusion of the analyte into the MIP and NIP coatings of the respective BPEs.

The green LED emission was recorded on a Fujifilm X-H2–1050 camera with a Fujinon XF16–80 mm F4-R-OIS-WR lens. Digital camera pictures of the LED were taken after the incubation period every 0.5 s for 20 s, allowing determination of the LED emission intensity once it had stabilized (a stable intensity of the green light occurred around the 30th picture). Photographic images were processed with Image J 1.54 software.

2.4.2. Microfluidic platform

The microfluidic cell was built as follows: a PVC (polyvinyl chloride) template was designed and in-house manufactured (UCM Research Support Facilities) to produce a 55 mm × 6 mm × 2 mm microfluidic channel, in which the hybrid BPE is placed. Then, two methacrylate bars (17 mm × 2 mm × 2 mm) were glued to the PVC template to create the corresponding cavities for the feeders upon demolding. The template was glued to the bottom of a 9-cm plastic Petri dish and 27.4 g of the SYLGARD™ 184 mixture of PDMS elastomer and curing agent (9:1 w/w), previously centrifuged to remove any dissolved air, was carefully added. Once cured for 48 h at 40 °C, the solid elastomer was removed from the Petri dish and cut into a rectangular shape (77 mm × 32 mm × 5 mm), and the graphite feeders were mechanically inserted into the generated cavities. The resulting PDMS BE channel was attached to a standard microscope slide to which the Au/LED/Au@MIP device is fixed by means of a double-sided tape (Kapton). The PDMS/glass slide assembly was sandwiched between two drilled PMMA (polymethylmethacrylate) plates (89 mm × 45 mm × 8 mm) and tightened with four butterfly nuts (Figure S3). The top PMMA plate featured a threaded opening to attach a SMA905-terminated optical fiber patchcord (StellarNet F1000-UV-VIS-SR 1000-µm 1-m PVC-coated PCS silica fiber) that carries the LED light to the spectrometer. The latter is a USB-powered Ocean Optics FLAME-S-VIS-NIR-ES fiberoptic spectrometer equipped with a 200 µm entrance slit, a 600 lines mm⁻¹ 350–1000 nm grating and a 2048-pixel Sony ILX511B linear CCD sensor. The

measurements were acquired in the presence of ambient light.

The microfluidic measurements were performed by injecting 600 µL of the working electrolytic solution, containing the desired analyte concentration ($0 \leq [\text{ZON}] \leq 2000 \text{ ng mL}^{-1}$; $0 \leq [\text{DON}] \leq 100 \text{ ng mL}^{-1}$), into the chamber by means of a plastic 1-mL syringe punctured into the PDMS between the feeder cathode and the bare Au wire. Additionally, another plastic syringe barrel with a needle was placed between the feeder anode and the Au@MIP wire as the liquid sample outlet. The injected solution volume is incubated for 5 min before applying a constant electric field (1.8 V cm⁻¹) between the feeders (placed 4.9 cm apart, Figure S3). Collection of the LED light spectrum by the spectrometer (15 s integration time, 10-point boxcar width, “dark electrical mode” selected) is launched 5 s after the electric field has been applied to the feeders. The emission spectrum was analyzed with SSPS SigmaPlot 14.0 software.

3. Results and discussion

3.1. Synthesis and characterization of the MIP-coated gold wire

The ZON-selective MIP was obtained by following a reported procedure [10]. Therefore, we have not carried out any further optimization of the monomer composition, monomers/template ratio or reaction conditions. In brief, it is prepared by thermal polymerization of a EAMA/CDHB/MAM/EDMA monomer mixture in a 2:1:2:20 mol ratio in DMSO on the surface of a gold disk electrode previously functionalized with acrylamide groups (Figure S1). As a first proof of the chemical modification, the surface morphology of the obtained MIP-coated, NIP-coated and the pristine Au electrodes was examined by scanning electron microscopy (SEM) (Figure S4). The SEM micrographs reveal a smooth homogeneous surface for the unmodified gold wire, whereas the polymer-modified surfaces exhibit a rough morphology corroborating their polymer coating. It is important to highlight that, due to the limited magnification of the microscope, a clear distinction of the morphological differences between the MIP and NIP surfaces cannot be achieved.

After the surface characterization we studied the electrochemical behavior of the polymer coating (*vide infra* and Figure S5). As such, the MIP and NIP behave as classical insulators, hence limiting the electron transfer rate constants between the Au surface and the electroactive probes ([Fe(CN)₆]³⁻ and [Fe(CN)₆]⁴⁻). In a first approximation, this fact leads to a decrease of the current passing through the LED with concomitant dim light emission. However, we hypothesize that the binding of the target mycotoxin to the polymer sites induces a reconfiguration of the MIP network, thereby facilitating the interfacial electron transfer reaction. This suggestion aligns with the so-called “gate effect”, which establishes that the binding of a target analyte to the polymer recognition sites leads to significant structural modifications of the polymer matrix [49]. The MIP nature plays a crucial role in determining the specific changes that may occur. For instance, one mechanism involves shrinkage of the polymer network due to the exchange between solvent molecules and the analyte. As the functional groups in the selective MIP cavities interact closely with the complementary ones of the analyte, a slight contraction of the polymer backbone occurs. This shrinkage facilitates the formation of pathways that allow the redox probe to reach the electrode surface more easily, eventually increasing the current signal (Figure S6). This effect highlights the critical importance of structural reconfiguration in molecularly imprinted polymers during the analyte detection, as emphasized in various studies [50,51].

To support this explanation, the voltammetric behavior of the [Fe(CN)₆]^{3-/4-} redox pair was investigated separately with a pristine Au disk, a MIP- and a NIP-coated electrode. This study was carried out in a classic three-electrode cell containing 0.1 mol L⁻¹ phosphate buffer (pH 8.2), [Fe(CN)₆]³⁻ and [Fe(CN)₆]⁴⁻ (5 mmol L⁻¹ each), in the absence and in the presence of ZON (1000 ng mL⁻¹). As it can be observed in Figure S5A, a diffusion-limited quasi-reversible process with a $\Delta E_p \sim 180 \text{ mV}$ was measured with the pristine Au electrode, both in the

absence and in the presence of ZON, demonstrating that the mycotoxin of interest is not electroactive within the selected range of potential. This is in agreement with the reported behavior of ZON under similar experimental conditions [52]. Hence, the analyte does not contribute to the Faradaic current quantified by our electrochemical setup. However, in the absence of the mycotoxin, the current associated with the redox process decreases ca. 4-fold after coating the gold electrode surface with either the MIP or the NIP (Figure S5B and S5C). Nevertheless, an increase in the current density of the redox process was observed in the presence of ZON (Figure S5B and S5C), with this enhancement being more pronounced in the case of the MIP-coated electrode (Figure S5B). This fact suggests that the presence of ZON within the MIP matrix facilitates the diffusion of the electroactive redox probe towards the electrode surface and, consequently, the electron transfer reactions. This effect is similar to the “gate effect” mentioned above, where the permeability of certain types of MIPs is modulated by specific interactions with their target molecules. Furthermore, it has been shown that the presence of the target analyte significantly alters the surface roughness of MIPs, indicating changes in polymer structure [53]. Such alterations can lead to an expansion of the pores, thereby enhancing the diffusion of redox probes through the polymer to the electrode surface. This effect ultimately boosts the Faradaic current response, as observed here in the presence of the target analyte. Additionally, a higher current density was observed with the MIP-coated than with the NIP-coated electrode, both in the absence and presence of ZON. This difference can be attributed to the distinct local porosity and accessible surface area of the MIP, which are influenced by the incorporation of the template molecule during its synthesis [54,55].

3.2. Classical BE platform for the wireless quantification of ZON

Having demonstrated the effect of the mycotoxin on the electron transfer features of the MIP-modified electrode, we adapted such an analyte-dependent process to the wireless BE with LED transduction format. For both the Au@MIP and Au@NIP hybrid BPEs, we fabricated polymer-coated Au wire electrodes and connected each of them to the anode of a miniature green LED (see Experimental section), while a bare Au wire was connected to each LED cathode. Considering the intrinsic threshold potential of the green LED declared by the manufacturer (~2.1 V) and the overall length of the BPEs ($l = 4$ cm), electric field values above 0.52 V cm^{-1} would be required to switch the LED on (Eq. S1). In principle, under these conditions, the polarization potential difference (ΔV) of the hybrid BPE would enable the oxidation and reduction of a redox probe at the anodic and cathodic extremities of the device, respectively. As a consequence, the concomitant electron flow should produce a high enough current to trigger the LED emission. However, larger electric field values are actually required due to the intrinsic low conductivity of the solution and the interfacial resistive contribution of the polymer layer. This can be readily addressed by using redox probes requiring a relatively small ΔV such as the $[\text{Fe}(\text{CN})_6]^{3-/4-}$ redox pair (~0.18 V, Figure S5). In this way, by applying an adequate electric field between the feeder electrodes, we can provoke the LED emission in the presence of the mycotoxin since the redox reactions will take place, while its emission will not occur in the absence of the mycotoxin due to inhibition of the redox process (Fig. 2).

As discussed above, binding of the mycotoxin to the MIP facilitates the access of the redox probe to the Au wire due to the polymer shrinking that leads to pore widening (Figure S6). Furthermore, it is reasonable to think that such pore widening may be related to the amount of mycotoxin bound to the MIP. In order to corroborate this hypothesis, the radiance power of the LEDs connected to either the hybrid Au@MIP or the Au@NIP BPEs as a function of ZON concentration was evaluated (Fig. 2). To this end, each ensemble was placed at the center of a BE cell (Figure S2) containing the electrolytic working solution. Under these conditions, the LED in each BPE remains off in the absence of ZON (Fig. 2, inset). However, after the first analyte addition (10 ng mL^{-1}),

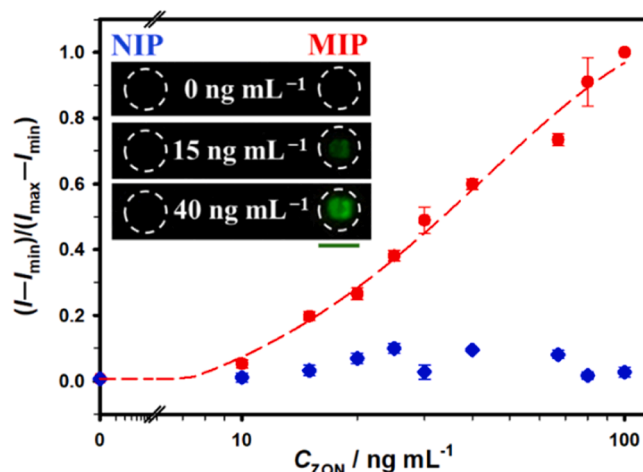


Fig. 2. Normalized emission of the LED as a function of the ZON concentration in aqueous 5 mmol L^{-1} phosphate buffer (pH 8.2) solution in the presence of both $[\text{Fe}(\text{CN})_6]^{3-}$ and $[\text{Fe}(\text{CN})_6]^{4-}$ (0.8 mmol L^{-1} each) subject to a constant electric field of 1.16 V cm^{-1} for the hybrid Au@MIP (red dots) and Au@NIP BPEs (blue diamonds). Inset: photographs of the green LED light generated by the Au@MIP and Au@NIP BPEs under those conditions, at the indicated ZON concentrations. The green bar below the LED indicates the scale, corresponding to 1.7 mm.

the LED connected to the Au@MIP switches on, whereas the Au@NIP LED remains off. These results are in agreement with the voltammetric measurement, lending additional support to the polymer “gate effect” caused by the ZON binding that facilitates the access of the redox probe to the electrode surface, allowing the electron transfer reactions there. The LED intensity as a function of the ZON concentration is plotted in Fig. 2. A correlation between the normalized light intensity and the amount of analyte present in the solution was obtained for the Au@MIP BPE (Fig. 2, red dots). On the contrary, the Au@NIP BPE remains off along the full range of concentrations tested (Fig. 2, blue diamonds), corroborating the key role of the selective recognition element.

Having demonstrated the essential function of the MIP in the occurrence of the bipolar electrochemical process, we studied the system specificity, i.e. the light-emitting behavior of the device in the presence of a potentially interfering species such as deoxynivalenol (DON), another habitual mycotoxin. ZON and DON are currently the most common mycotoxins found in contaminated food worldwide [15]. Moreover, both mycotoxins originate from the same fungus and share similar functional groups and molecular size (Fig. 3). Therefore, selective quantification of ZON in the presence of such a molecule is highly desirable. The effect of DON on the composite Au@MIP electrode was tested under the same conditions than those used for the ZON analysis. The selected mycotoxins concentration range ($0 \leq [\text{ZON}] \leq 100 \text{ ng mL}^{-1}$; $0 \leq [\text{DON}] \leq 500 \text{ ng mL}^{-1}$) is based on the maximum residue limits (MRLs) established by the European Commission Regulation (EU) 2023/915 for each mycotoxin in different foods. As can be observed in Fig. 3, the LED in the BPE remains off in the absence of both ZON and DON. Unexpectedly, a gradual increase of the LED intensity as a function of the DON concentration was also observed. This behavior suggests the existence of nonspecific interactions between the imprinted polymer and DON that occur during the incubation period. However, higher concentrations of DON ($> 30 \text{ ng mL}^{-1}$) than those of ZON ($> 5 \text{ ng mL}^{-1}$) are required to trigger the LED emission (Fig. 3). Furthermore, a steeper increase of the latter was observed with the additions of ZON compared to the DON pattern. The slope of the linear section of the light intensity–concentration plots is related to the binding constant of the analyte to the MIP coating. In this regard, it is evident that the binding of ZON to the MIP is more efficient than the interaction of DON as the slope of the plot for the former mycotoxin ($2 \times 10^{-2} \text{ mL ng}^{-1}$) is

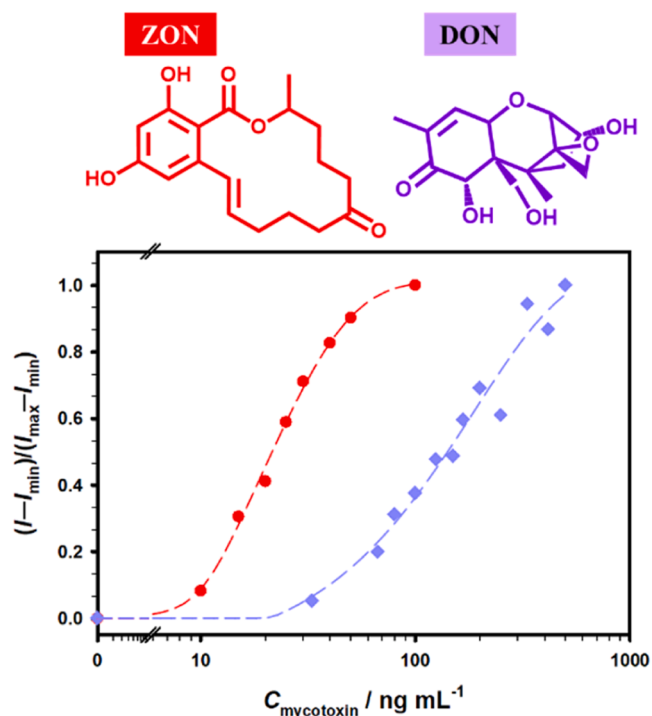


Fig. 3. (Top) Chemical structures of the ZON and DON toxins. (Bottom) Normalized LED light intensity as a function of the ZON (red dots) or DON (purple diamonds) concentration, in 5 mmol L⁻¹ aqueous phosphate buffer (pH 8.2) solution, in the presence of both [Fe(CN)₆]³⁻ and [Fe(CN)₆]⁴⁻ (0.8 mmol L⁻¹ each) at a constant electric field of 1.16 V cm⁻¹ with a composite Au@MIP BPE.

one order of magnitude larger than the slope for the potential interferent ($3 \times 10^{-3} \text{ mL ng}^{-1}$). Nonetheless, the interference of DON would only occur at a concentration higher than ca. 30 ng mL⁻¹ based on the LED switch-on effect of this mycotoxin (Fig. 3). Based on these results, a new cell design was developed to reduce nonspecific interactions, decrease the working sample volumes, and streamline the LED intensity monitoring, thus optimizing the detection of ZON in the presence of potential interferents.

3.3. Microfluidic platform for the wireless quantification of ZON

After identifying significant differences in the response of the Au@MIP sensor to related mycotoxins, we decided to design a microfluidic setup to fulfill our goals. For this purpose, a microfluidic cell was

fabricated using PDMS and equipped with a channel to place the Au/LED/Au@MIP BPE and two graphite bars embedded at its ends as feeder electrodes; further details can be found in the Experimental section and Figure S3. To perform a measurement, the electrolytic solution containing the analyte is injected into the PDMS chamber, incubated, and then subjected to an electric field, after which the LED emission spectrum is recorded using a fiberoptic spectrometer. Under these conditions, the successive injection/removal of the solutions mimics a dynamic approach that minimizes the nonspecific interactions. Fig. 4 illustrates the BE measurements of ZON solutions taken in the microfluidic cell. It must be noted that the applied electric field is higher in the microfluidic setup than in the classical system due to geometric considerations. The use of a spectrometer rather than a camera or a photodiode allows to collect a full spectrum of the green light emitted by the transducing LED (Fig. 4 A). This spectrum is centered at $(577 \pm 1) \text{ nm}$ and its maximum intensity and area depend on the mycotoxin concentration. From these spectra, a plot of the normalized area under the emission curve ($(S - S_{\min}) / (S_{\max} - S_{\min})$) as a function of the ZON concentration was built (Fig. 4B).

In the same way we observed for the classical BE cell, the LED remains off in the absence of the mycotoxin whereas it begins to emit from the first addition of ZON (10 ng mL⁻¹). A linear correlation between the normalized emission area and the ZON concentration was obtained in the 10–70 ng mL⁻¹ concentration range ($r^2 = 0.993$) (Fig. 4B), with a low detection limit of 3 ng mL⁻¹. At high concentrations of ZON (> 100 ng mL⁻¹), a decrease of the LED emission occurs (Fig. 4 C and Figure S7). Such a decrease suggests that the MIP has reached saturation of its binding sites, and the excess of mycotoxin binds unspecifically to the polymer surface. This unspecific binding at high ZON concentration interferes with the electron-transfer process leading to a depletion of the electron flux across the LED and to the concomitant decrease of its emission. Naturally, this unspecific binding should affect one or more properties of the MIP; otherwise, the signal would level off and not decrease.

Considering that the high limit of detection depends on the saturation of the MIP binding sites, the way to raise it would be to escalate the number of binding sites by increasing the amount of MIP on the gold wire. In order to keep the current response time of the sensor, the latter goal might be realized by either using a thicker gold wire (since the electric field required to trigger the oxidation and reduction at each extremity of the bipolar electrode, Eq. S1, does not depend on the electrode thickness), or nanostructuring the gold wire before applying the MIP coating.

Having demonstrated the functionality and simplicity of the microfluidic system for MIP-based BE measurements, we investigated the effect of DON on this setup. The optical behavior of the Au/LED/Au@MIP device was assessed under the same experimental conditions at different

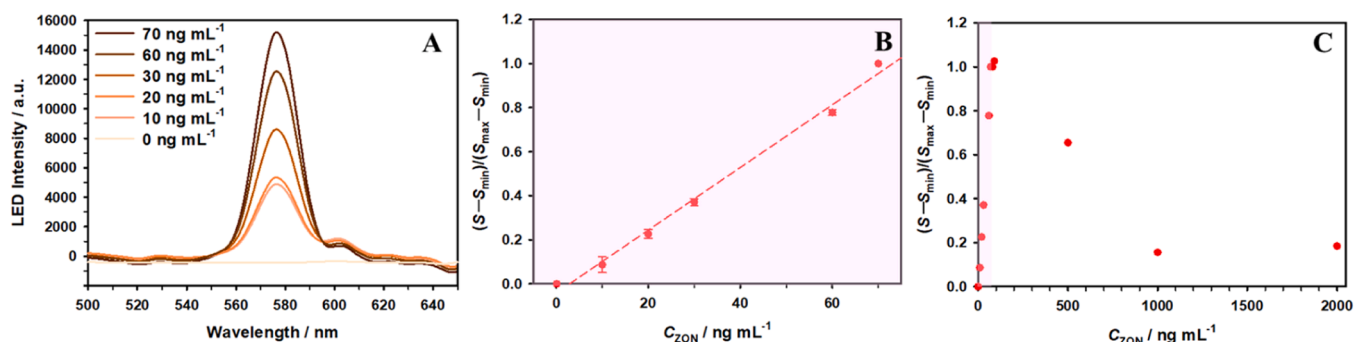


Fig. 4. (A) LED light spectra measured by the spectrometer as a function of the ZON concentration (0–70 ng mL⁻¹) in 5 mmol L⁻¹ aqueous phosphate buffer (pH 8.2) solution, in the presence of both [Fe(CN)₆]³⁻ and [Fe(CN)₆]⁴⁻ (0.8 mmol L⁻¹ each) at a constant electric field of 1.8 V cm⁻¹ with a microfluidic Au/LED/Au@MIP BE cell. (B) Normalized area under the emission spectrum as a function of the ZON concentration obtained from the spectral data in Fig. 4 A. The red dashed line represents the best fit to the equation $y = -0.04 + 0.01x$. (C) Normalized area under the emission spectrum as a function of the ZON concentration in the 0–2000 ng mL⁻¹ concentration range.

concentrations of DON. In the 0–70 ng mL⁻¹ range, we observe a linear response of the device to ZON. Remarkably, no LED emission was observed after adding DON in this concentration range (Fig. 5). The slopes of the sensor response to ZON (1.4×10^{-2} mL ng⁻¹) and DON (4.3×10^{-5} mL ng⁻¹) evidence that the microfluidic device efficiently minimizes the nonspecific interactions of the analyte with the MIP, enhancing the method selectivity by three orders of magnitude with respect to the BE classical system. Furthermore, the reusability of the electrodes was demonstrated by performing repeated measurements with the device for at least three times during one month, with no loss of the analytical signal. It is important to point out that, before each series of experiments, the polymer-coated wires were stored at 5 °C in ACN and, prior to its use washed for 30 min with a MeOH–TFA solution (95:5 v/v) followed by another 30 min with MeOH to remove residual TFA.

Finally, the results obtained with the microfluidic platform and the classic BE setup were successfully compared using the elliptical joint confidence region (EJCR) plot derived from the ordinary least squares regression analysis (Figure S8) [56].

4. Conclusions

For the first time, a light-emitting device based on a hybrid molecularly imprinted polymer (MIP)-Au material for the wireless electrochemical analysis of ZON, a widespread mycotoxin, has been successfully fabricated. This novel system capitalizes on the molecular recognition ability of the MIP and its electrochemical transduction through an analyte-mediated “gate effect”. Furthermore, owing to the optical readout provided by a micro-LED, the convenience of microfluidics, and the fundamental principles of BE, the optosensing device is compact, fast and versatile.

The microfluidic platform will readily allow automation through a flow injection analytical (FIA) system. The latter would enable to introduce washing steps after the incubation of the MIP-coated electrode with the sample in order to minimize even further the nonspecific interactions between the analyte and the recognition element. As far as the device components are concerned, the PDMS cell might be replaced with alternative materials such as the thermoplastic elastomer Flexdym™, a multiblock copolymer of polystyrene/ethylene-butylene/polystyrene for improved flexibility, easy molding and bonding. The green LED could be changed for a red LED to take advantage of their stronger radiance power and higher sensitivity of the solid-state detectors in this region. Moreover, a simple photodiode with an amplification circuit might be substituted for the current compact spectrometer and optical fiber to lower the cost of the BE-based device. Further work is in progress to use the novel Au/LED/Au@MIP device to perform the wireless electroanalysis of other mycotoxins in real-world food samples, thus addressing a significant global health concern.

CRediT authorship contribution statement

Moya-Cavas Tamara: Writing – review & editing, Writing – original draft, Methodology, Investigation, Data curation, Conceptualization. **Orellana Guillermo:** Writing – review & editing, Writing – original draft, Supervision, Methodology, Investigation, Conceptualization. **Salinas Gerardo:** Writing – review & editing, Writing – original draft, Investigation, Formal analysis, Conceptualization. **Benito-Peña Elena:** Writing – review & editing, Investigation. **Arias-Aranda Leslie R.:** Methodology, Conceptualization. **Sojic Neso:** Writing – review & editing, Supervision, Funding acquisition, Formal analysis. **Bouffier Laurent:** Writing – review & editing.

Declaration of Competing Interest

The authors declare the following personal relationships which may be considered as potential competing interests: Guillermo Orellana was

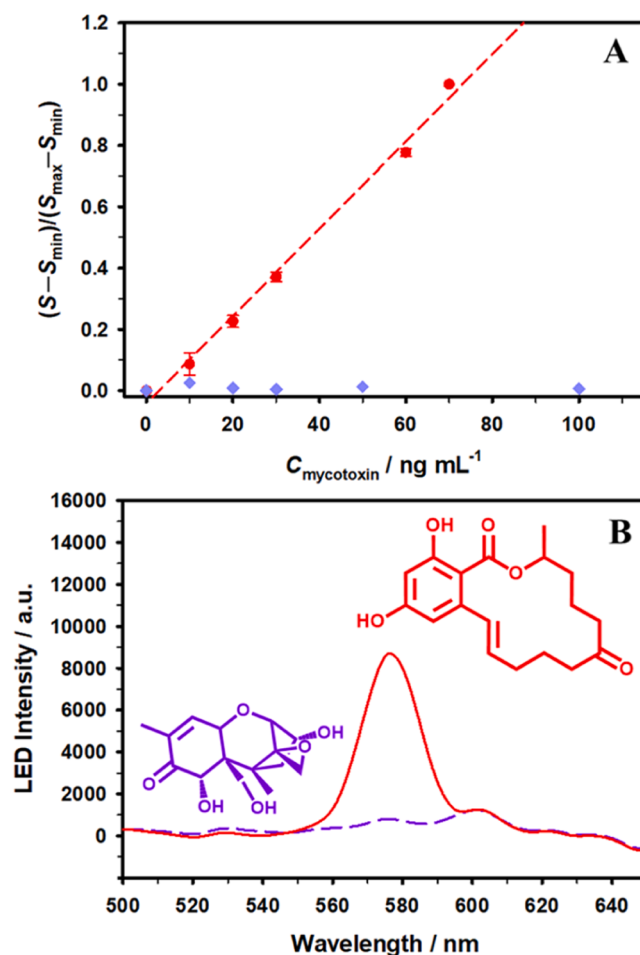


Fig. 5. (A) Normalized emission area as a function of the ZON (red dots) and DON (purple diamonds) concentrations, measured in a 5 mmol L⁻¹ phosphate buffer (pH 8.2) aqueous solution in the presence of both [Fe(CN)₆]³⁻ and [Fe(CN)₆]⁴⁻ (0.8 mmol L⁻¹ each) at a constant electric field (1.8 V cm⁻¹) with a hybrid Au@MIP BPE. (B) LED emission spectra recorded at a ZON concentration of 30 ng mL⁻¹ (red line) and DON concentration of 30 ng mL⁻¹ (purple dashed line) under the same experimental conditions.

previously co-Editor-in-Chief of Sensors & Actuators B: Chem. If there are other authors, they declare that they have no known competing financial interests or personal relationships that could have appeared to influence the work reported in this paper.

Acknowledgements

This work has been funded by grant PID2021–127457OB-C21/22 funded by MICIU/AEI/10.13039/501100011033 and by ERDF “A way of making Europe”. T.M.C. thanks grant PRE2019–089433 funded by MICIU/AEI/10.13039/501100011033 and by ESF “Investing in your future”. L. R. A.-A. acknowledges the University of Bordeaux for her PhD scholarship. N.S. thanks the European Union (Grant agreement No. 101135402, Mobiles project) for financial support.

Appendix A. Supporting information

Supplementary data associated with this article can be found in the online version at [doi:10.1016/j.snb.2025.137566](https://doi.org/10.1016/j.snb.2025.137566).

Data availability

Data will be made available on request.

References

- [1] M.C. Moreno-Bondi, E. Benito-Peña, T.D. Moya-Cavas, J.U. Ruiz, Molecularly Imprinted Polymer-Based Biomimetic Sensors for Food Analysis. *Encyclopedia of Sensors and Biosensors*, Elsevier, 2023, pp. 568–598, <https://doi.org/10.1016/B978-0-12-822548-6.00105-9>.
- [2] K. Haupt, P.X. Medina Rangel, B.T.S. Bui, Molecularly Imprinted Polymers: Antibody Mimics for Bioimaging and Therapy, *Chem. Rev.* 120 (17) (2020) 9554–9582, <https://doi.org/10.1021/acs.chemrev.0c00428>.
- [3] J.J. BelBruno, Molecularly Imprinted Polymers, *Chem. Rev.* 119 (1) (2019) 94–119, <https://doi.org/10.1021/acs.chemrev.8b00171>.
- [4] R. Wang, L. Wang, J. Yan, D. Luan, sun Tao, J. Wu, X. Bian, Rapid, Sensitive and Label-Free Detection of Pathogenic Bacteria Using a Bacteria-Imprinted Conducting Polymer Film-Based Electrochemical Sensor, *Talanta* 226 (2021) 122135, <https://doi.org/10.1016/j.talanta.2021.122135>.
- [5] W. Huang, Y. Liu, N. Wang, G. Song, X. Yin, L. Zhang, X. Ni, W. Xu, A Sensitive Electrochemical Sensor Based on Ion Imprinted Polymers with Gold Nanoparticles for High Selective Detecting Cd (II) Ions in Real Samples, *J. Inorg. Organomet. Polym.* 31 (5) (2021) 2043–2053, <https://doi.org/10.1007/s10904-021-01892-8>.
- [6] P. Cornelis, S. Givanoudi, D. Yongabi, H. Iken, S. Duwé, O. Deschaume, J. Robbins, P. Dedecker, C. Bartic, M. Wübbenhorst, M.J. Schöning, M. Heyndrickx, P. Wagner, Sensitive and Specific Detection of *E. Coli* Using Biomimetic Receptors in Combination with a Modified Heat-Transfer Method, *Biosens. Bioelectron.* 136 (2019) 97–105, <https://doi.org/10.1016/j.bios.2019.04.026>.
- [7] J. Quílez-Alburquerque, A.B. Descalzo, M.C. Moreno-Bondi, G. Orellana, Luminescent Molecularly Imprinted Polymer Nanocomposites for Emission Intensity and Lifetime Rapid Sensing of Tenuazonic Acid Mycotoxin, *Polymer* 230 (2021) 124041, <https://doi.org/10.1016/j.polymer.2021.124041>.
- [8] M. Cieplak, W. Kutner, Artificial Biosensors: How Can Molecular Imprinting Mimic Biorecognition? *Trends Biotechnol.* 34 (11) (2016) 922–941, <https://doi.org/10.1016/j.tibtech.2016.05.011>.
- [9] A.G. Marroquín-Cardona, N.M. Johnson, T.D. Phillips, A.W. Hayes, Mycotoxins in a Changing Global Environment – A Review, *Food Chem. Toxicol.* 69 (2014) 220–230, <https://doi.org/10.1016/j.fct.2014.04.025>.
- [10] T. Moya-Cavas, F. Navarro-Villoslada, J. Lucas Urraca, L. Antonio Serrano, G. Orellana, M. Cruz Moreno-Bondi, Simultaneous Determination of Zearalenone and Alternariol Mycotoxins in Oil Samples Using Mixed Molecularly Imprinted Polymer Beads, *Food Chem.* 412 (2023) 135538, <https://doi.org/10.1016/j.foodchem.2023.135538>.
- [11] T. Sergeyeva, D. Yarynka, E. Piletska, R. Linnik, O. Zaporozhets, O. Brovko, S. Piletsky, El'skaya, A. Development of a Smartphone-Based Biomimetic Sensor for Aflatoxin B1 Detection Using Molecularly Imprinted Polymer Membranes, *Talanta* 201 (2019) 204–210, <https://doi.org/10.1016/j.talanta.2019.04.016>.
- [12] J.G. Pacheco, M. Castro, S. Machado, M.F. Barroso, H.P.A. Nouws, C. Delerue-Matos, Molecularly Imprinted Electrochemical Sensor for Ochratoxin A Detection in Food Samples, *Sens. Actuators B* 215 (2015) 107–112, <https://doi.org/10.1016/j.snb.2015.03.046>.
- [13] R. Weiss, M. Freudenschuss, R. Krška, B. Mizaikoff, Improving Methods of Analysis for Mycotoxins: Molecularly Imprinted Polymers for Deoxynivalenol and Zearalenone, *Food Addit. Contam.* 20 (4) (2003) 386–395, <https://doi.org/10.1080/0265203031000065827>.
- [14] X. Han, B. Huangfu, T. Xu, W. X. C. Asakiya, K. Huang, X. He, Research Progress of Safety of Zearalenone: A Review, *Toxins* 14 (6) (2022) 386, <https://doi.org/10.3390/toxins14060386>.
- [15] *Mycotoxin Risk Management App*. (<https://www.dsm.com/anh/products-and-services/tools/mycotoxin-contamination/mycotoxin-risk-management-app.html>) (accessed 2024-08-26).
- [16] M. Pascale, A. De Girolamo, A. Visconti, N. Magan, I. Chianella, E.V. Piletska, S. A. Piletsky, Use of Itaconic Acid-Based Polymers for Solid-Phase Extraction of Deoxynivalenol and Application to Pasta Analysis, *Anal. Chim. Acta* 609 (2) (2008) 131–138, <https://doi.org/10.1016/j.aca.2008.01.004>.
- [17] M. Jiang, M. Braiek, A. Florea, A. Chrouda, C. Farre, A. Bonhomme, F. Bessueille, F. Vocanson, A. Zhang, N. Jaffrezic-Renault, Aflatoxin B1 Detection Using a Highly-Sensitive Molecularly-Imprinted Electrochemical Sensor Based on an Electropolymerized Metal Organic Framework, *Toxins* 7 (9) (2015) 3540–3553, <https://doi.org/10.3390/toxins7093540>.
- [18] J. Jodlbauer, N.M. Maier, W. Lindner, Towards Ochratoxin A Selective Molecularly Imprinted Polymers for Solid-Phase Extraction, *J. Chromatogr. A* 945 (1–2) (2002) 45–63, [https://doi.org/10.1016/S0021-9673\(01\)01504-7](https://doi.org/10.1016/S0021-9673(01)01504-7).
- [19] D. Bueno, R.K. Mishra, A. Hayat, G. Catanante, V. Sharma, R. Muñoz, J.-L. Marty, Portable and Low Cost Fluorescence Set-up for in-Situ Screening of Ochratoxin A, *Talanta* 159 (2016) 395–400, <https://doi.org/10.1016/j.talanta.2016.06.039>.
- [20] N. Karimian, P. Hashemi, A. Afkhami, H. Bagheri, The Principles of Bipolar Electrochemistry and Its Electroanalysis Applications, *Curr. Opin. Electrochem.* 17 (2019) 30–37, <https://doi.org/10.1016/j.coelec.2019.04.015>.
- [21] S.E. Fosdick, K.N. Knust, K. Scida, R.M. Crooks, Bipolar Electrochemistry, *Angew. Chem. Int. Ed.* 52 (40) (2013) 10438–10456, <https://doi.org/10.1002/anie.201300947>.
- [22] L. Koefoed, S.U. Pedersen, K. Daasbjerg, Bipolar Electrochemistry—A Wireless Approach for Electrode Reactions, *Curr. Opin. Electrochem.* 2 (1) (2017) 13–17, <https://doi.org/10.1016/j.coelec.2017.02.001>.
- [23] A.J. Robinson, C. McBeth, R. Rahman, R.J.M. Hague, F.J. Rawson, Bipolar Electrochemical Growth of Conductive Microwires for Cancer Spheroid Integration: A Step Forward in Conductive Biological Circuitry, *Sci. Rep.* 14 (1) (2024) 21012, <https://doi.org/10.1038/s41598-024-71236-2>.
- [24] C. Qin, Z. Yue, G.G. Wallace, J. Chen, Bipolar Electrochemical Stimulation Using Conducting Polymers for Wireless Electroceuticals and Future Directions, *ACS Appl. Bio Mater.* 5 (11) (2022) 5041–5056, <https://doi.org/10.1021/acsbm.2c00679>.
- [25] E. Villani, S. Inagi, Electrosynthesis with Split-Bipolar Electrodes, *Curr. Opin. Electrochem.* 44 (2024) 101443, <https://doi.org/10.1016/j.coelec.2024.101443>.
- [26] N. Shida, Y. Zhou, S. Inagi, Bipolar Electrochemistry: A Powerful Tool for Electrifying Functional Material Synthesis, *Acc. Chem. Res.* 52 (9) (2019) 2598–2608, <https://doi.org/10.1021/acs.accounts.9b00337>.
- [27] N. Shida, E. Villani, M. Sanuki, K. Miyamoto, A. Gotou, T. Isogai, A. Yamauchi, T. Fuchigami, I. Tomita, S. Inagi, Bipolar Electrochemical Fluorination of Triphenylmethane and Bis(Phenylthio)Diphenylmethane Derivatives in a U-Shaped Cell, *Electrochem* 89 (5) (2021) 476–479, <https://doi.org/10.5796/electrochemistry.21-00074>.
- [28] L. Bouffier, D. Zigah, N. Sojic, A. Kuhn, Bipolar (Bio)Electroanalysis, *Annu. Rev. Anal. Chem.* 14 (14, 2021) 65–86, <https://doi.org/10.1146/annurev-anchem-090820-093307>.
- [29] K.L. Rahn, R.K. Anand, Recent Advancements in Bipolar Electrochemical Methods of Analysis, *Anal. Chem.* 93 (1) (2021) 103–123, <https://doi.org/10.1021/acs.analchem.0c04524>.
- [30] X. Zhang, L. Zhang, Q. Zhai, W. Gu, J. Li, E. Wang, Self-Powered Bipolar Electrochromic Electrode Arrays for Direct Displaying Applications, *Anal. Chem.* 88 (5) (2016) 2543–2547, <https://doi.org/10.1021/acs.analchem.6b00054>.
- [31] S. Arnaboldi, G. Salinas, G. Bonetti, R. Cirilli, T. Benincori, A. Kuhn, Bipolar Electrochemical Rotors for the Direct Transduction of Molecular Chiral Information, *Biosens. Bioelectron.* 218 (2022) 114740, <https://doi.org/10.1016/j.bios.2022.114740>.
- [32] A. dePoulpiquet, B. Diez-Buitrago, M. Milutinovic, B. Goudeau, L. Bouffier, S. Arbault, A. Kuhn, N. Sojic, Dual-Color Electrogenerated Chemiluminescence from Dispersions of Conductive Microbeads Addressed by Bipolar Electrochemistry, *ChemElectroChem* 3 (3) (2016) 404–409, <https://doi.org/10.1002/celec.201500402>.
- [33] H. Li, L. Bouffier, S. Arbault, A. Kuhn, C.F. Hogan, N. Sojic, Spatially-Resolved Multicolor Bipolar Electrochemiluminescence, *Electrochem. Commun.* 77 (2017) 10–13, <https://doi.org/10.1016/j.elecom.2017.02.006>.
- [34] A.L. Dauphin, A. Akkach, S. Voci, A. Kuhn, G. Xu, L. Bouffier, N. Sojic, Tracking Magnetic Rotating Objects by Bipolar Electrochemiluminescence, *J. Phys. Chem. Lett.* 10 (18) (2019) 5318–5324, <https://doi.org/10.1021/acs.jpcclett.9b02188>.
- [35] Y. Wang, R. Jin, N. Sojic, D. Jiang, H. Chen, Intracellular Wireless Analysis of Single Cells by Bipolar Electrochemiluminescence Confined in a Nanopipette, *Angew. Chem. Int. Ed.* 59 (26) (2020) 10416–10420, <https://doi.org/10.1002/anie.202002323>.
- [36] L.R. Arias-Aranda, G. Salinas, H. Li, C.F. Hogan, A. Kuhn, L. Bouffier, N. Sojic, Annihilation Electrochemiluminescence Triggered by Bipolar Electrochemistry, *ChemElectroChem* (2024) e202400522, <https://doi.org/10.1002/celec.202400522>.
- [37] H. Xing, X. Zhang, Q. Zhai, J. Li, E. Wang, Bipolar Electrode Based Reversible Fluorescence Switch Using Prussian Blue/Au Nanoclusters Nanocomposite Film, *Anal. Chem.* 89 (7) (2017) 3867–3872, <https://doi.org/10.1021/acs.analchem.7b00246>.
- [38] G. Salinas, S.M. Beladi-Mousavi, L. Gerasimova, L. Bouffier, A. Kuhn, Wireless Imaging of Transient Redox Activity Based on Bipolar Light-Emitting Electrode Arrays, *Anal. Chem.* 94 (41) (2022) 14317–14321, <https://doi.org/10.1021/acs.analchem.2c02872>.
- [39] X. Qin, J. Gao, H.-J. Jin, Z.-Q. Li, X.-H. Xia, Closed Bipolar Electrode Array for Optical Reporting Reaction-Coupled Electrochemical Sensing and Imaging, *Chem. - Eur. J.* 29 (8) (2023) e202202687, <https://doi.org/10.1002/chem.202202687>.
- [40] W. Zhao, Y. Ma, J. Ye, Development of a Novel Sensing Platform Based on Molecularly Imprinted Polymer and Closed Bipolar Electrochemiluminescence for Sensitive Detection of Dopamine, *J. Electroanal. Chem.* 888 (2021) 115215, <https://doi.org/10.1016/j.jelechem.2021.115215>.
- [41] C. Li, M. Feng, D. Stanković, L. Bouffier, F. Zhang, Z. Wang, N. Sojic, Wireless Rotating Bipolar Electrochemiluminescence for Enzymatic Detection, *Analyst* 149 (9) (2024) 2756–2761, <https://doi.org/10.1039/D4AN00365A>.
- [42] B. Gupta, P. Suchomski, A. Ashwin Melvin, S. Linfield, M. Opallo, W. Nogala, Optical Readout of Moisture in Sand Employing Bipolar Electrochemistry, *Electrochem. Commun.* 140 (2022) 107329, <https://doi.org/10.1016/j.elecom.2022.107329>.
- [43] X. Zhang, C. Chen, J. Yin, Y. Han, J. Li, E. Wang, Portable and Visual Electrochemical Sensor Based on the Bipolar Light Emitting Diode Electrode, *Anal. Chem.* 87 (9) (2015) 4612–4616, <https://doi.org/10.1021/acs.analchem.5b01018>.
- [44] M. Liu, L.R. Arias-Aranda, H. Li, L. Bouffier, A. Kuhn, N. Sojic, G. Salinas, Wireless Multimodal Light-Emitting Arrays Operating on the Principles of LEDs and ECL, *ChemPhysChem* 25 (12) (2024) e202400133, <https://doi.org/10.1002/cphc.202400133>.
- [45] Y. Boukarkour, S. Reclusa, N. Sojic, A. Kuhn, G. Salinas, Wireless Light-Emitting Electrode Arrays for the Evaluation of Electrocatalytic Activity, *Chem. - Eur. J.* 30 (29) (2024) e202400078, <https://doi.org/10.1002/chem.202400078>.
- [46] G. Salinas, G. Bonetti, R. Cirilli, T. Benincori, A. Kuhn, S. Arnaboldi, Wireless Light-Emitting Device for the Determination of Chirality in Real Samples, *Electrochim. Acta* 421 (2022) 140494, <https://doi.org/10.1016/j.electacta.2022.140494>.
- [47] G. Salinas, L. Bouffier, N. Sojic, A. Kuhn, Light-Emitting Bipolar Electrochemistry: A Straightforward Way to Illustrate Thermodynamic Aspects to Students, *J. Solid State Electrochem.* 28 (3) (2024) 1225–1231, <https://doi.org/10.1007/s10008-023-05690-9>.

- [48] D.A. Bui, P.C. Hauser, Analytical Devices Based on Light-Emitting Diodes – a Review of the State-of-the-Art, *Anal. Chim. Acta* 853 (2015) 46–58, <https://doi.org/10.1016/j.aca.2014.09.044>.
- [49] P.S. Sharma, A. Garcia-Cruz, M. Cieplak, K.R. Noworyta, W. Kutner, Gate Effect' in Molecularly Imprinted Polymers: The Current State of Understanding, *Curr. Opin. Electrochem.* 16 (2019) 50–56, <https://doi.org/10.1016/j.coelec.2019.04.020>.
- [50] T. Alizadeh, M. Akhondian, M.R. Ganjali, A Ferrocene/Imprinted Polymer Nanomaterial-Modified Carbon Paste Electrode as a New Generation of Gate Effect-Based Voltammetric Sensor, *N. J. Chem.* 42 (6) (2018) 4719–4727, <https://doi.org/10.1039/C7NJ03396F>.
- [51] Y. Yoshimi, K. Sato, M. Ohshima, E. Piletska, Application of the 'Gate Effect' of a Molecularly Imprinted Polymer Grafted on an Electrode for the Real-Time Sensing of Heparin in Blood, *Analyst* 138 (17) (2013) 5121–5128, <https://doi.org/10.1039/C3AN00909B>.
- [52] A.-E. Radi, A. Eissa, T. Wahdan, Molecularly Imprinted Impedimetric Sensor for Determination of Mycotoxin Zearalenone, *Electroanalysis* 32 (8) (2020) 1788–1794, <https://doi.org/10.1002/elan.201900528>.
- [53] Y. Yoshimi, R. Ohdaira, C. Iiyama, K. Sakai, "Gate Effect" of Thin Layer of Molecularly-Imprinted Poly(Methacrylic Acid-Co-Ethyleneglycol Dimethacrylate), *Sens. Actuators B: Chem.* 73 (1) (2001) 49–53, [https://doi.org/10.1016/S0925-4005\(00\)00671-7](https://doi.org/10.1016/S0925-4005(00)00671-7).
- [54] G. Neusser, S. Eppler, J. Bowen, C.J. Allender, P. Walther, B. Mizaikoff, C. Kranz, FIB and MIP: Understanding Nanoscale Porosity in Molecularly Imprinted Polymers via 3D FIB/SEM Tomography, *Nanoscale* 9 (38) (2017) 14327–14334, <https://doi.org/10.1039/C7NR05725C>.
- [55] T. Renkecz, G. Mistlberger, M. Pawlak, V. Horváth, E. Bakker, Molecularly Imprinted Polymer Microspheres Containing Photoswitchable Spiropyran-Based Binding Sites, *ACS Appl. Mater. Interfaces* 5 (17) (2013) 8537–8545, <https://doi.org/10.1021/am401958e>.
- [56] M.C. Ortiz, M.S. Sánchez, L.A. Sarabia, Quality of Analytical Measurements: Univariate Regression, in: S. Brown, R. Tauler, B. Walczak (Eds.), *Comprehensive Chemometrics (Second Edition)*, Elsevier, Oxford, 2020, pp. 71–105, <https://doi.org/10.1016/B978-0-12-409547-2.14869-3>.

Tamara Moya Cavas holds a B.Sc. and a M.Sc. degree in Chemistry from the University of Murcia (Spain). She is currently pursuing her PhD in the Department of Analytical Chemistry at the Complutense University of Madrid (Spain), as part of the *Optical Chemosensors & Applied Photochemistry* research group (GSOLFA) led by Prof. Guillermo Orellana. Her primary research focuses on the development of (bio)mimetic materials for the creation of optical sensors and analytical separations aimed at analyzing mycotoxins in food products.

Leslie R. Arias-Aranda holds a B.Sc. and a M.Sc. degree in Chemistry from the National Autonomous University of Mexico (UNAM). She is currently pursuing her PhD at the Institute of Molecular Sciences (ISM) at the University of Bordeaux (France). She works under the supervision of Dr. Laurent Bouffier and Prof. Neso Sojic in the Analytical

Nanosystems research group (NSYSA). Her research interests focus on analytical electrochemistry, electrochemiluminescence, and bipolar electrochemistry.

Elena Benito-Peña did her PhD in Chemistry from Complutense University of Madrid (Spain). After completing her postdoctoral studies at Tufts University, she became a Tenured Professor in the Department of Analytical Chemistry at UCM. She leads the Analytical Chemistry section of the UCM *Optical Chemosensors & Applied Photochemistry* research group (GSOLFA). Her research focuses on developing optical-based biosensing platforms, creating novel recognition elements (e.g., molecularly imprinted polymers, biomimetic peptides, recombinant antibodies, and luminescent proteins), and applying these technologies to clinical, food, and environmental fields for detecting substances like mycotoxins, drugs, biomarkers, and antibiotics.

Laurent Bouffier graduated from the University of Grenoble (France) where he also obtained his PhD in 2005. He moved to the University of Liverpool (UK) as a postdoctoral research associate before being appointed by the *Centre National de la Recherche Scientifique* (CNRS) in 2010. He is affiliated to the Institute of Molecular Sciences (ISM) at the University of Bordeaux (France). His research activities focus on bipolar electrochemistry, electrogenerated chemiluminescence and opto-electrochemistry.

Neso Sojic obtained a Ph.D. in electrochemistry from the Université Pierre et Marie Curie (Paris, France). After postdoctoral studies at the University of Texas at Dallas, he joined the faculty at the University of Bordeaux (France). He is Associate Editor of the journal: *Chemical & Biomedical Imaging*. His main research interests are in electrochemiluminescence, analytical electrochemistry, microscopy and fiber-optic sensors.

Gerardo Salinas received his Master and PhD degrees in electrochemistry from the National Autonomous University of Mexico (UNAM). Since 2018 he is performing postdoctoral studies at the Institute of Molecular Sciences (ISM) at the University of Bordeaux (France) under the supervision of Prof. Alexander Kuhn. His research interests include analytical electrochemistry, bipolar electrochemistry, conducting polymers, electrochemistry-based light emitting devices and magneto-electrochemistry.

Guillermo Orellana is Full Professor of Organic Chemistry and Photochemistry at Complutense University of Madrid (UCM) in Spain, received his PhD in Chemistry from the same University, and was a Fulbright Postdoctoral Scholar at Columbia University in the City of New York in Prof. N.J. Turro group. He leads the multidisciplinary UCM *Optical Chemosensors & Applied Photochemistry* Group (GSOLFA). His research interests include novel photochemical principles for optical chemical sensing, molecular engineering of indicator dyes, molecular recognition (nano)materials, fiber-optic chemical sensors and biosensors and optoelectronic instrumentation for environmental monitoring, (bio)process analysis, and aerospace. He boasts a long-standing collaboration with industrial partners and the transfer of research results through agreements, authoring many international and national patents.